Characteristics and modifying factors of asbestos-induced oxidative DNA damage

Li Jiang,[1,2] Hirotaka Nagai,[1,2] Hiroki Ohara,[1,2] Shigeo Hara,[1] Mitsuhiro Tachibana,[1,3] Seishiro Hirano,[4] Yasushi Shinohara,[5] Norihiko Kohyama,[6] Shinya Akatsuka[1,2] and Shinya Toyokuni[1,2,7]

[1]Department of Pathology and Biology of Diseases, Graduate School of Medicine, Kyoto University, Yoshida-Konoe-cho, Sakyo-ku, Kyoto 606-8501; [2]Department of Pathology and Biological Responses, Graduate School of Medicine, Nagoya University, 65 Tsurumai-cho, Showa-ku, Nagoya 466-8550; [3]Department of Diagnostic Pathology, Graduate School of Medicine, Kyoto University, Shogoin-Kawahara-cho, Sakyo-ku, Kyoto 606-8501; [4]Research Center for Environmental Risk, National Institute for Environmental Studies, 16-2 Onogawa, Tsukuba 305-8506; [5]National Institute of Occupational Health and Safety, 6-21-1 Nagao, Tama-ku, Kawasaki 214-8585; [6]National Science Laboratory, Faculty of Economics, Toyo University, 5-28-20, Hakusan, Bunkyo-ku, Tokyo 112-8606, Japan

(Received June 20, 2008/Revised July 16, 2008/Accepted July 22, 2008/Online publication September 4, 2008)

Respiratory exposure to asbestos has been linked with mesothelioma in humans. However, its carcinogenic mechanism is still unclear. Here we studied the ability of chrysotile, crocidolite and amosite fibers to induce oxidative DNA damage and the modifying factors using four distinct approaches. Electron spin resonance analyses revealed that crocidolite and amosite containing high amounts of iron, but not chrysotile, catalyzed hydroxyl radical generation in the presence of H_2O_2, which was enhanced by an iron chelator, nitrilotriacetic acid, and suppressed by desferal. Natural iron chelators, such as citrate, adenosine 5′-triphosphate and guanosine 5′-triphosphate, did not inhibit this reaction. Second, we used time-lapse video microscopy to evaluate how cells cope with asbestos fibers. RAW264.7 cells, MeT-5 A and HeLa cells engulfed asbestos fibers, which reached not only cytoplasm but also the nucleus. Third, we utilized supercoiled plasmid DNA to evaluate the ability of each asbestos to induce DNA double strand breaks (DSB). Crocidolite and amosite, but not chrysotile, induced DNA DSB in the presence of iron chelators. We cloned the fragments to identify break sites. DSB occurred preferentially within repeat sequences and between two G:C sequences. Finally, i.p. administration of each asbestos to rats induced not only formation of nuclear 8-hydroxy-2′-deoxyguanosine in the mesothelia, spleen, liver and kidney but also significant iron deposits in the spleen. Together with the established carcinogenicity of i.p. chrysotile, our data suggest that asbestos-associated catalytic iron, whether constitutional or induced by other mechanisms, plays an important role in asbestos-induced carcinogenesis and that chemoprevention may be possible through targeting the catalytic iron. (*Cancer Sci* 2008; 99: 2142–2151)

Asbestos fibers have been heavily used in industry from World War II to the present because of their durability, heat-resistance and low cost.[1,2] However, in 1987, the International Agency for Research on Cancer (IARC) designated asbestos fibers as a group I (definite) carcinogen for humans (http://monographs.iarc.fr/ENG/Classification/crthgr01.php), and asbestos fibers were banned in many European and North American countries in the 1990s.[1,2] In June of 2005, asbestos-associated deaths suddenly attracted social attention in Japan because it was reported that 79 people who worked in factories using asbestos had been killed by an asbestos-associated rare cancer called diffuse malignant mesothelioma (DMM) over the past 26 years.[3] Furthermore, people who lived near those factories also suffered from the same fatal disease.[4] The characteristics of DMM are as follows: (i) it is associated with repeated asbestos exposure;[5,6] (ii) once diagnosed, prognosis is poor;[7] and (iii) it takes 30–40 years after the start of asbestos exposure for DMM to occur.[5,6] It is expected that the incidence of DMM in Japan will peak in 2025 with 100 000 predicted deaths from this neoplasm.[8]

There are several hypotheses about the pathogenesis of DMM, which may be summarized as follows: (i) the 'oxidative stress theory'[9] is based on the fact that asbestos fibers are foreign bodies and that epidemiological studies show that asbestos fibers that contain iron (a transition metal which catalyzes free radical generation) are more carcinogenic;[10] (ii) the 'chromosome tangling theory' postulates that asbestos fibers damage chromosomes when cells divide;[11] (iii) the 'theory of adsorption of many specific proteins as well as carcinogenic molecules' states that asbestos *in vivo* contains chemicals including cigarette smoke components;[9] and (iv) the 'SV40 oncogenic virus contamination theory' (polio vaccination)[1] does not appear to be relevant, at least in Japan.[12,13]

In the pathological diagnosis, the presence of asbestos (ferruginous) bodies is a hallmark of asbestos exposure. Indeed, excess iron is carcinogenic not only to animals, but also to humans.[14,15] In the present paper, we describe novel characteristics and modifying factors for asbestos-associated oxidative DNA damage.

Materials and Methods

Asbestos and animals. International Union Against Cancer (UICC) asbestos fibers (chrysotile A, crocidolite and amosite) were suspended in physiological saline (5 mg/mL) and autoclaved for injection into rats or exposure to cell lines. Detailed composition and size analyses of these asbestos fibers were reported previously.[16] The asbestos suspension was sonicated for 30 min immediately before use to prevent aggregation of the fibers. Twenty one 8-week-old specific pathogen-free male Wistar rats (Shizuoka Laboratory Animal Center, Shizuoka, Japan) were divided into seven groups of three animals each and were subjected to a single i.p. injection of 10 mg asbestos into each rat unless they were used as untreated controls. The animals were killed 1 or 4 weeks after administration. Their organs were collected for histological and immunohistochemical analyses.

Scanning electron microcopy. Asbestos fibers were imaged with a Hitachi S-4700 cold-field emission scanning electron microscope (SEM) operated at 1 kV. Element spectra were obtained using energy dispersive X-ray spectroscopy (EDS, Super Xerophy, EMAX-5770; Horiba) attached to SEM.

Electron spin resonance spectral measurement. Electron spin resonance (ESR) spectra were measured with an ESR spectrometer (FR30; JEOL, Tokyo, Japan) according to a previously described method,[17,18] with some modifications. The instrument settings were as follows: standard first derivative mode with 100 kHz modulation, a modulation amplitude of 0.079 mT; scanning width 10 mT, center magnetic field 339.5 mT; microwave power and frequency of 4 mW/9.425 GHz; a scanning time of 2 min with a time constant of 0.30 s at a temperature of 290.0 K. The relative height of the lowest field line against an internal standard,

[7]To whom correspondence should be addressed.
E-mail: toyokuni@med.nagoya-u.ac.jp

doi: 10.1111/j.1349-7006.2008.00934.x

$Mn_{(3)}$, was recorded. The spectrum of the spin-trapped signals produced upon addition of 90 mM hydrogen peroxide to $FeSO_4$ (100 μg/mL), silica (100 μg/mL), chrysotile A (100 μg/mL), crocidolite (100 μg/mL) or amosite (100 μg/mL) in the presence of 50 mM 5,5′-dimethyl-1-pyrroline-1-oxide (DMPO) and 50 mM phosphate-buffered saline (PBS) were recorded after the solution was incubated at room temperature for 1.5 min following DMPO addition. RDC-60-S disposable syringes (Radical Research, Tokyo, Japan) were used for measurements. Nitrilotriacetic acid disodium salt (NTA) was from Nacalai Tesque (Kyoto, Japan) and all the other iron chelators were from Sigma (St. Louis, MO, USA). Iron chelators were added to a final concentration of 100 μM.

Cell culture conditions. The RAW264.7, HeLa and MeT-5A cell lines were obtained through the American Type Culture Collection (Manassas, VA, USA). The FRCC562 cell line was established from a ferric nitrilotriacetate-induced rat renal cell carcinoma.[19] The RAW264.7 and HeLa cells were maintained in Dulbecco's modified Eagle's medium (Gibco, Rockville, MD, USA) supplemented with 10% fetal bovine serum (FBS) under 5% CO_2 in air at 37°C. MeT-5 A cells were maintained in Medium 199 containing Earle's balanced salt solution and 0.75 mM L-glutamine supplemented with 1.25 g/L sodium bicarbonate, 10 ng/mL epidermal growth factor, 400 nM hydrocortisone, 870 nM zinc-free bovine insulin, 20 mM HEPES, trace elements B liquid from Mediatech (Manassas) and 10% FBS under 5% CO_2 in air at 37°C.

Electron spin resonance measurement of cells. For direct ESR measurement of RAW264.7 cells, cells were plated at a density of 1.0×10^4 cell/well in 96-well plates and were grown for 16 h before asbestos treatment. The cells were incubated in the medium after addition of each type of asbestos at a different concentration (1, 3, 5 and 10 μg/cm^2) for 12 h at 37°C. In some samples, H_2O_2 was added to a final concentration of 1 mM and incubated for 30 min. Cells were washed with PBS three times to remove extracellular asbestos fibers, followed by collection of the cells after trypsinization (20 μL). The conditions for ESR were the same as those for asbestos fibers described above. RDC-60-S disposable syringes (Radical Research) were used for measurements.

3-(4,5-dimethylthiazol-2-yl)-2,5-diphenyltetrazolium bromide assay. Cell viability was quantified by 3-(4,5-dimethylthiazol-2-yl)-2,5-diphenyltetrazolium bromide (MTT; Sigma) assay. Cells were plated at a density of 0.8 (for MeT-5 A) or 1.0 (for RAW264.7, FRCC562 or HeLa) $\times 10^4$ cells/well in 96-well tissue culture plates and grown at least 16 h before treatment. The cells were incubated in the medium with or without various concentrations of asbestos. In the case of RAW264.7 cells, experiments were also performed adding H_2O_2 at a final concentration of 1 mM. At the end of the incubation, MTT was added to the medium at a final concentration of 0.4 mg/mL. The plates were incubated at 37°C for 1 h. The medium was removed and replaced with 100 μL dimethylsulfoxide to dissolve the purple dye in each well. The absorbance was measured in an Optimax microplate reader at a wavelength of 570 nm with background subtraction at 690 nm.

Imaging of living cells and hydroxyphenyl fluorescein fluorescence assay. Living cells were imaged with or without 5 μM hydroxyphenyl fluorescein (HPF) as probes. Asbestos fibers (5 μg/cm^2) were added onto cells 24 h after plating on 35-mm collagen-coated glass-bottomed dishes. The cells were imaged with an Olympus IX70 inverted microscope equipped with an image splitter, DualView (Optical Insights, Santa Fe, NM, USA) and an electron multiplying charge-coupled device (CCD) camera, iXon DV887 (Andor Technology, Belfast, UK). The imaging process was controlled by MetaMorph software (Molecular Devices, Sunnyvale, CA, USA). In some experiments, cells were imaged with an Olympus IX81 inverted microscope equipped with a laser-based autofocusing system, IX2-ZDC, and an automatically programmable XY stage, MD-XY30100T-Meta, which allowed us to obtain the time-lapse images of several view fields in a single experiment. Fluorescent images were obtained by the inverted microscope (Zeiss, Oberkochen, Germany), or the inverted epifluorescence microscopy of IX71 and IX81 microscope (Olympus, Tokyo, Japan), equipped with an Orca II CCD camera (Hamamatsu Photonics, Hamamatsu, Japan), processed and analyzed by MetaMorph software.

Monoclonal antibodies. Monoclonal antibody N45.1 recognizing 8-hydroxy-2′-deoxyguanosine (8-OHdG)[20,21] was used.

Histological and immunohistochemical analyses. The tissues were fixed with 10% neutral formalin solution. After dehydration, tissue specimens were subjected to paraffin embedding, cut to a 3-μm thickness and stained with hematoxylin–eosin. For immunohistochemical analyses, the avidin–biotin complex method with peroxidase was used as described previously.[20]

Analysis of DNA strand breaks. An expression vector plasmid, pcDEF3 (6094 bp),[22] was amplified with TOP10 cells (Invitrogen, Carlsbad, CA, USA). Plasmid DNA (0.5 μg) in 10 mM PBS, pH 7.4, was incubated at 24°C for 15 min with different combinations of substances in a total volume of 20 μL under ambient oxygen pressure. Plasmid DNA and phosphate buffer were pretreated with Chelex resin in the sodium form (Sigma) (20%, v/v) to minimize metal contamination. Asbestos (100 μg/mL), silica (100 μg/mL) or iron salts (0.25 mM $FeCl_3$ or $FeCl_2$), H_2O_2 (0.25 mM) with or without iron chelating agent (1 mM) were pipetted into different parts of a tube. The reaction was started by centrifugation and stopped by the addition of 2 μL of 100 mM deferoxamine mesylate. All incubations were terminated at the same time. DNA strand breaks were evaluated by 0.8–1.0% agarose gel electrophoresis using untreated DNA as a control as previously described.[23,24] For the linear form (form III) that appeared most abundantly in the combination of crocidolite/amosite and nitrilotriacetic acid with H_2O_2, the DNA fragment was recovered from the gel, cloned with a TA or Zero blunt TOPO PCR cloning kit (Invitrogen) and sequenced with an ABI3130 genetic analyzer (Applied BioSystems, Foster City, CA, USA) for the identification of break sites.

Results

Physical analysis of UICC asbestos fibers. Scanning electron microscopic analyses showed that chrysotile fibers have curved, curly and wavy morphologies whereas crocidolite and amosite fibers are straight fibers with parallel sides and longitudinal grooves. Among the asbestos fibers, diameter and length differed considerably (Fig. 1a). Energy dispersive X-ray spectroscopy revealed that crocidolite and amosite contain abundant iron. Both fibers contained ferric and ferrous iron whereas amosite contained more ferrous iron.[16] Iron content in chrysotile was at the level of contamination on its surface (Fig. 1b).

Measurements of asbestos-induced free radicals in the presence of different iron chelators. ESR analyses showed that all the asbestos fibers generated hydroxyl radicals (1:2:2:1 signal) in the presence of H_2O_2 *in vitro*. Amosite was the strongest catalyst and crocidolite was also a strong catalyst whereas chrysotile was quite weak as a catalyst (Fig. 1c). We evaluated 12 different iron chelators for the modification of asbestos-catalyzed hydroxyl radical generation. NTA promoted hydroxyl radical generation catalyzed by all the asbestos. Diethylenetriaminepentaacetic acid (DTPA) and desferal were suppressive to all the reactions, but citrate was inhibitive only for the amosite-catalyzed reaction. Seven natural iron chelators of phosphate compounds were slightly inhibitory for the asbestos-catalyzed hydroxyl radical generation. This was especially noteworthy for amosite (Fig. 1d).

Asbestos-induced cellular toxicity *in vitro* and asbestos-catalyzed free radical generation in cells. Asbestos-induced cellular toxicity was detected in RAW264.7, FRCC562, HeLa and MeT-5 A cells using the MTT assay. The results indicated dose-dependent cellular toxicity in all the cell lines used whereas silica at the same

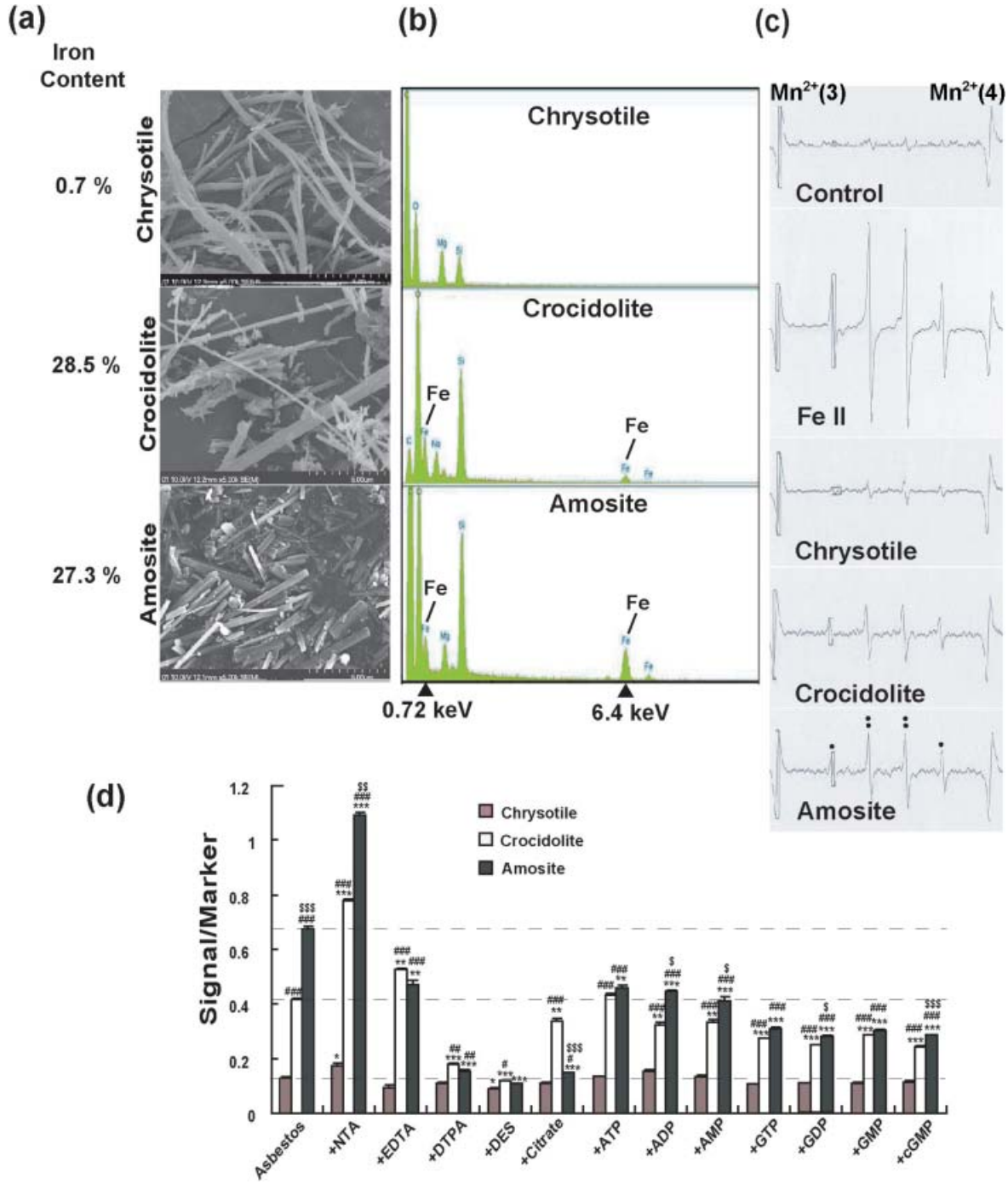

Fig. 1. Physicochemical features of asbestos and its modification by iron chelators. (a) Scanning electron microscopy images of chrysotile, crocidolite and amosite with different iron content (×5000). Each asbestos presented a different appearance. Iron content is from a reference paper.[26] (b) Energy dispersive X-ray spectroscopic spectrum of chrysotile, crocidolite and amosite. Crocidolite and amosite showed high content of iron. (c) Electron spin resonance (ESR) analyses of chrysotile, crocidolite and amosite in the presence of H_2O_2. Ferrous iron was used as positive control. The signals are those of hydroxyl radicals. (d) ESR analyses of chrysotile, crocidolite and amosite in the presence of H_2O_2 and different iron chelators. $n = 3$, means ± standard error of the mean; $^{*}P < 0.05$, $^{**}P < 0.01$, $^{***}P < 0.001$ vs each asbestos plus H_2O_2 alone; $^{\#}P < 0.05$, $^{\#\#}P < 0.01$, $^{\#\#\#}P < 0.001$ vs chrysotile plus H_2O_2 within each chelator group; $^{\$}P < 0.05$, $^{\$\$}P < 0.01$, $^{\$\$\$}P < 0.001$ vs crocidolite plus H_2O_2 within each chelator group. ADP, adenosine 5′-disphosphate; AMP, adenosine 5′-monophosphate; ATP, adenosine 5′-triphosphate; cGMP, cyclic guanosine monophosphate; DES, desferal; DTPA, diethylenetriaminepentaacetic acid; EDTA, ethylenediaminetetraacetic acid; GDP, guanosine 5′-diphosphate; GMP, guanosine 5′-monophosphate; GTP, guanosine 5′-triphosphate; NTA, nitrilotriacetic acid.

concentration did not show cytotoxicity. Among all the asbestos types, amosite was the most cytotoxic (Fig. 2a–d). For the RAW264.7 cell line, generation of hydroxyl radicals was measured with ESR after treatment with different concentrations of asbestos with or without H_2O_2 (Fig. 2e). The levels of hydroxyl radical signals were dose-dependent with crocidolite or amosite. The presence of H_2O_2 markedly enhanced the reaction. Chrysotile did not catalyze the generation of hydroxyl radical (Fig. 2e).

Cellular intake of asbestos fibers and hydroxyl radical generation in cells. Time-lapse video microscopy was used to study whether

doi: 10.1111/j.1349-7006.2008.00934.x

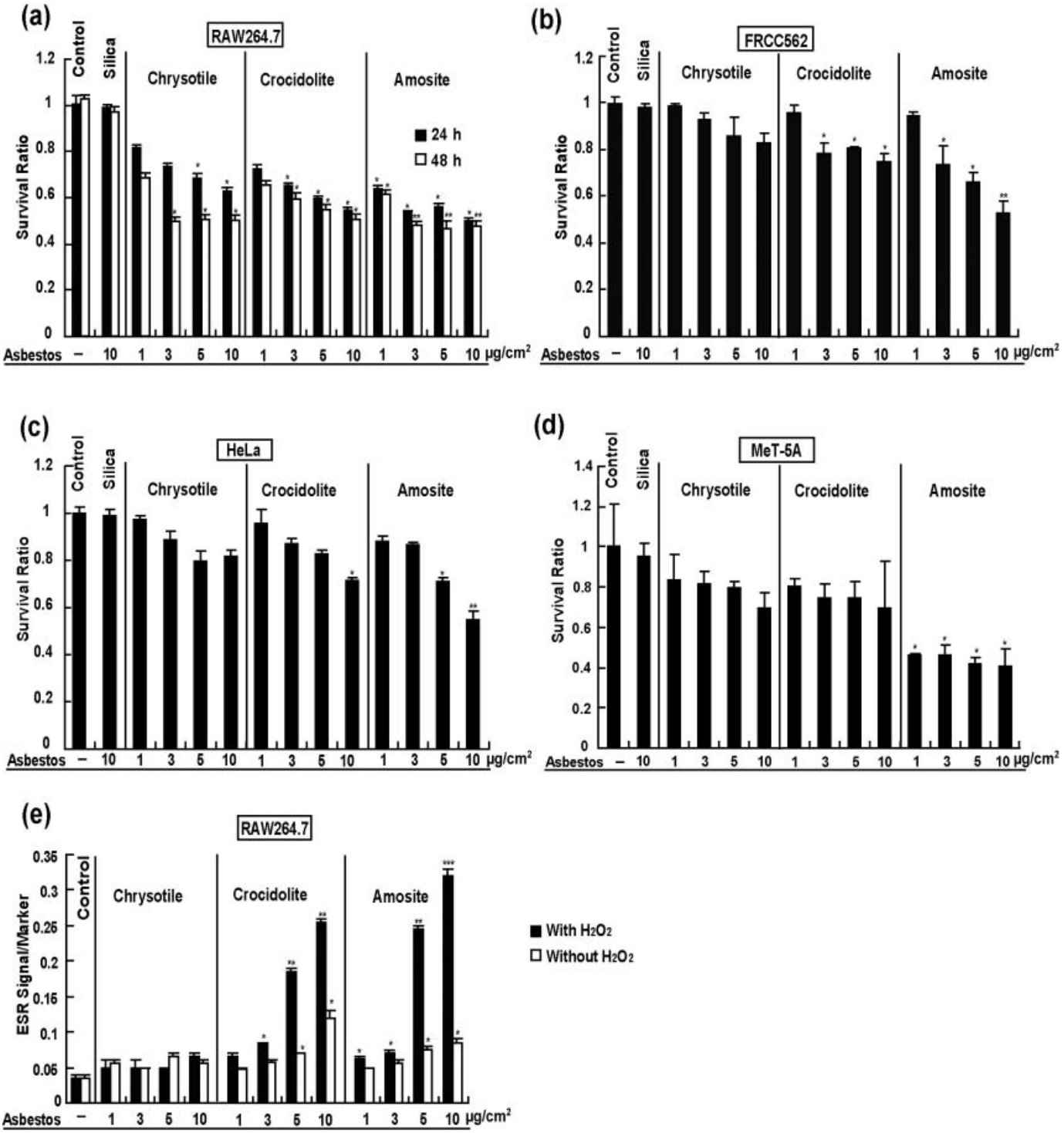

Fig. 2. Asbestos-induced cytotoxicity. Cell lines RAW264.7 (a), FRCC562 (b), HeLa (c) and MeT-5 A (d) were treated with different doses (1, 3, 5 and 10 μg/cm²) of chrysotile, crocidolite or amosite. Survival ratio was determined with 3-(4,5-dimethylthiazol-2-yl)-2,5-diphenyltetrazolium bromide assay. Electron spin resonance was determined by the use of RAW264.7 cell line after treatment with chrysotile, crocidolite or amosite with or without 1 mM H_2O_2 (e) ($n = 3$, mean ± standard error of the mean; $^*P < 0.05$, $^{**}P < 0.01$, $^{***}P < 0.001$ vs untreated control).

cells take up asbestos fibers and whether the cell–asbestos fiber interactions were associated with increased free radical generation and cellular toxicity. Four different cell lines were exposed to equal concentrations of crocidolite for 16 h, and the relative levels of HPF, a fluorescent sensor for hydroxyl radical generation, were recorded digitally. Not only RAW264.7 macrophage cells but also MeT-5A (non-transformed mesothelial cells), FRCC562 and HeLa cells (adenocarcinoma) took up crocidolite fibers, which not only reached the cytoplasm, but also eventually reached the nuclei (Fig. 3a and Suppl. video files). Fibers with relatively larger diameters and shorter lengths were engulfed earlier. We obtained similar results for chrysotile and amosite fibers (data not shown). Intake of crocidolite fibers was associated with cytoplasmic and nuclear generation of hydroxyl radicals (Fig. 3b).

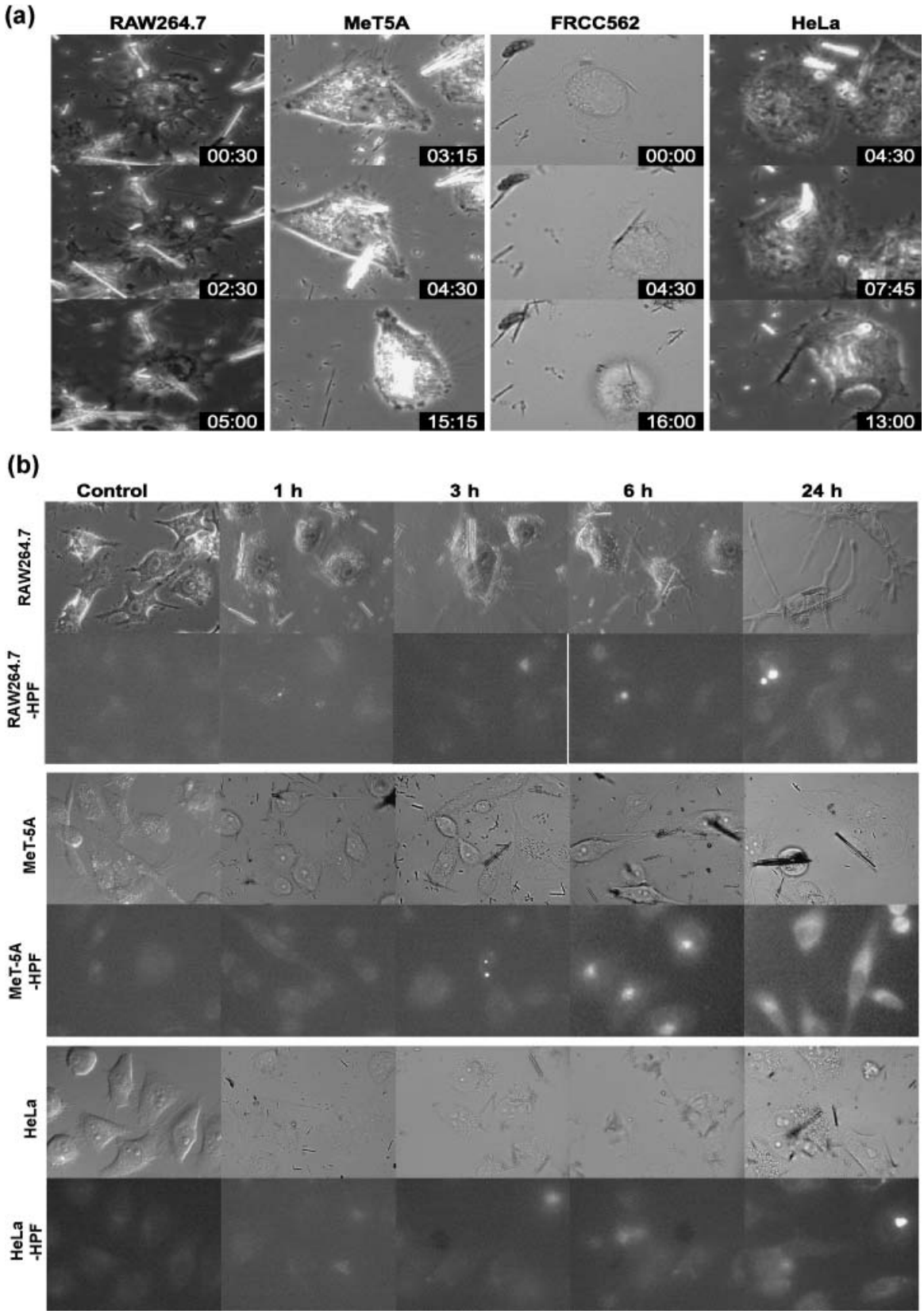

Fig. 3. Cellular intake of asbestos fibers and hydroxyl radical generation in cells. Four different cell lines, RAW264.7, FRCC562, HeLa and MeT-5 A, were incubated with 5 μg/cm^2 crocidolite for 14–16 h and during that time digital data were obtained every 15 min using time-lapse microscopy (a). Different kinds of cells engulfed one or more crocidolite fibers. Some of the fibers eventually reached the nuclei. The relative levels of hydroxyphenyl fluorescein were measured to determine whether hydroxyl radicals are generated through the intake of asbestos fibers (b). Representative data are shown.

doi: 10.1111/j.1349-7006.2008.00934.x

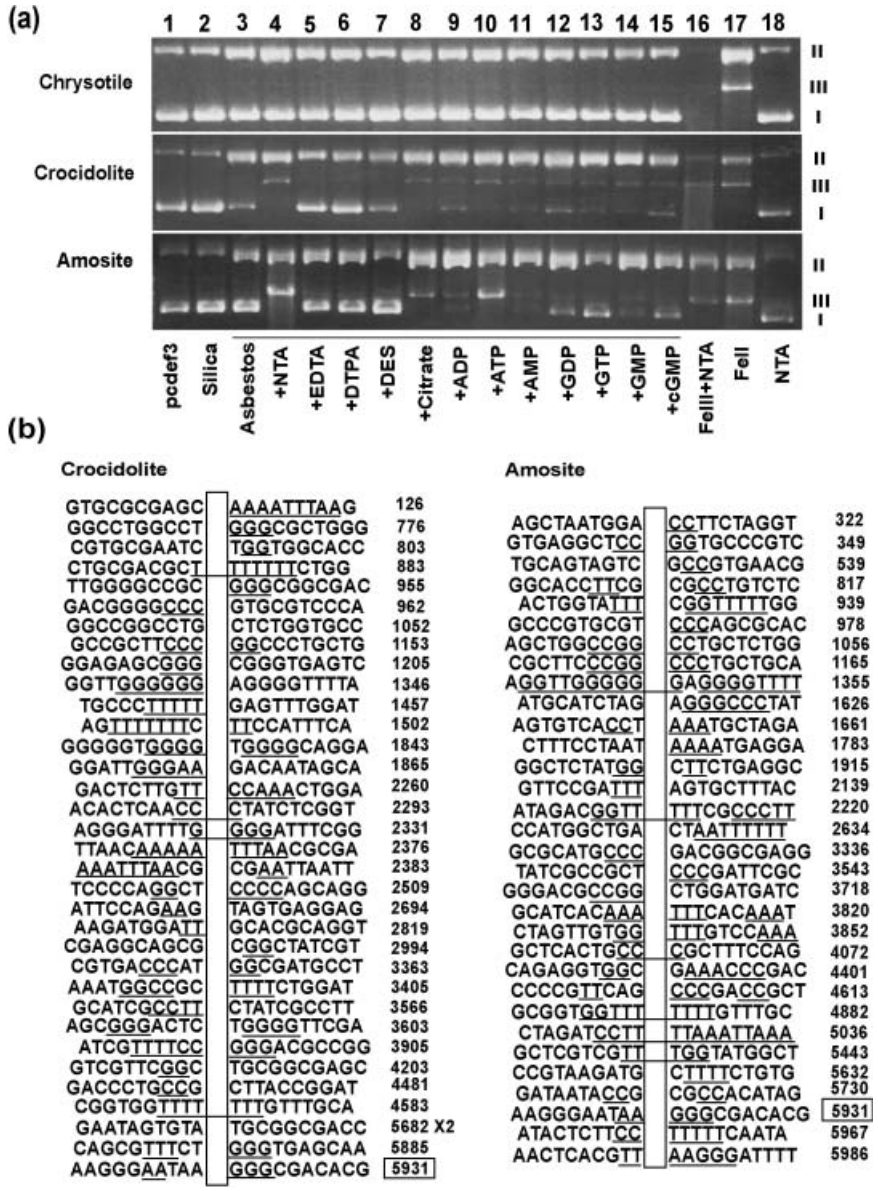

Fig. 4. Oxidative DNA breakage catalyzed by asbestos in the presence of H_2O_2 and its characteristics. Supercoiled plasmid DNA (pcDEF3 plasmid) was incubated with 100 μg/mL asbestos plus 0.25 mM H_2O_2 in the presence of various iron chelators for 15 min at 24°C and the reaction was stopped by addition of 2 μL of 100 mM deferoxamine mesylate. I, II and III indicate the positions of migrated supercoiled, circular and linear forms of plasmid DNA, respectively (a). The positions of double strand breaks were identified by cloning of the linear fragments and sequencing (b). ADP, adenosine 5′-disphosphate; AMP, adenosine 5′-monophosphate; ATP, adenosine 5′-triphosphate; cGMP, cyclic guanosine monophosphate; DES, desferal; DTPA, diethylenetriaminepentaacetic acid; EDTA, ethylenediaminetetraacetic acid; GDP, guanosine 5′-diphosphate; GMP, guanosine 5′-monophosphate; GTP, guanosine 5′-triphosphate; NTA, nitrilotriacetic acid.

Effect of iron chelators and sequence specificity on oxidative DNA breakage catalyzed by asbestos in the presence of H_2O_2. Because we observed that asbestos fibers eventually reached nuclei where they catalyzed hydroxyl radical generation, we decided to evaluate the sequence-specificity of DNA strand breaks in an *in vitro* model. Untreated plasmid DNA (pcDEF3 vector) showed a major band corresponding to the supercoiled form (form I) and a minor band corresponding to the nicked circular form (form II). No linear form (form III) was present in the untreated DNA. Plasmid DNA remained intact after incubation with 100 μg/mL silica and 0.25 mM H_2O_2 (Fig. 4a, lanes 1 and 2). However, when DNA was incubated with a mixture of 1 mM of different types of iron chelators and 100 μg/mL asbestos in the presence of 0.25 mM H_2O_2, strand breaks were produced as shown by the decrease in the amount of form I and the concomitant increase in form II (Fig. 4a, lanes 3–15). Though no significant form III was produced after addition of iron chelators in chrysotile, form III generation was evident with crocidolite or amosite in the presence of either NTA, citrate, adenosine 5′-disphosphate, adenosine 5′-triphosphate, adenosine 5′-monophosphate, guanosine 5′-diphosphate; guanosine 5′-monophosphate, guanosine 5′-triphosphate or cyclic guanosine monophosphate (Fig. 4a, lanes 4 and 8–15). In contrast, DTPA and desferal suppressed the reactions (Fig. 4a, lanes 6 and 7). These results indicate that not only the type of asbestos, but also the presence of iron chelators are important for the modulation of DNA strand breaks. To further investigate the characteristics of crocidolite- and amosite-induced DNA double strand breaks (DSB), we cloned linear DNA fragments (form III) induced by asbestos and NTA in the presence of H_2O_2, and sequenced them to identify the break sites in the plasmid DNA (Fig. 4b). Both crocidolite and amosite induced DSB preferentially within repeat sequences (74.3% crocidolite, $P < 0.005$ by χ^2-test; 78.1% amosite, $P < 0.001$ by χ^2-test vs 47.1% repeat sequence sites in pcDEF3) and between two G:C sequences (crocidolite, between A:T and A:T, 11.4%; between G:C and G:C, 34.3%; between A:T and G:C, 54.2%; amosite, between A:T and A:T, 28.1%; between G:C and G:C, 43.8%; between A:T and G:C, 28.2%, $P < 0.05$ by χ^2-test vs 1312 A; 1583 C; 1534 T; 1665 G; predicted between A:T and A:T, 21.8%; between G:C and G:C, 28.4%; between A:T and G:C, 49.8% in pcDEF3).

Histological alterations after i.p. administration of asbestos and asbestos-induced oxidative DNA damage. A single i.p. administration

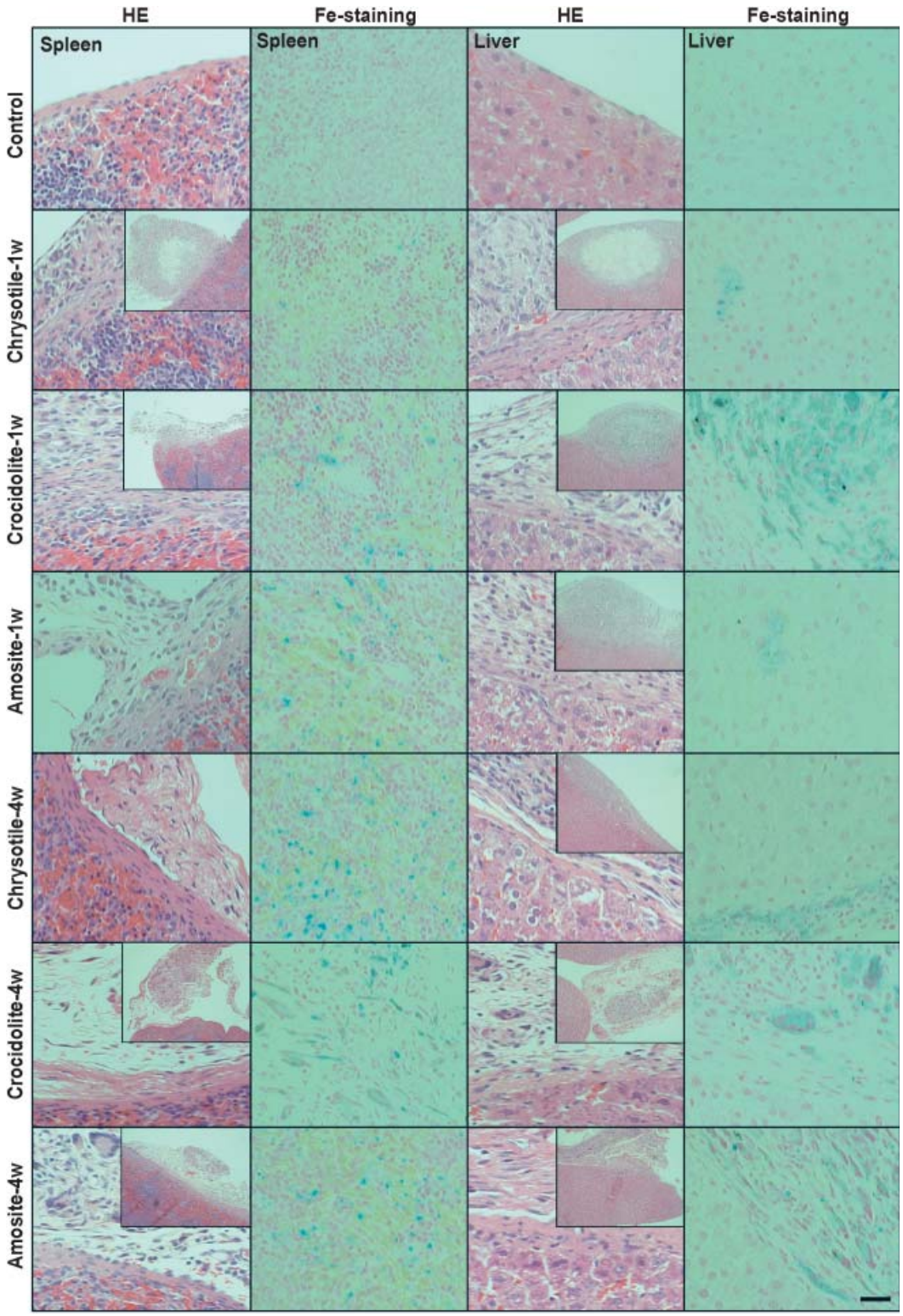

Fig. 5. Hematoxylin–eosin staining and Perl's iron staining after administration of asbestos. The surface of the spleen and liver after i.p. asbestos administration showed subserosal presence of asbestos fiber, granulomatous foreign body reaction and fibrosis. Especially, 4 weeks after administration, spleen treated with chrysotile showed marked iron deposition. (Scale line = 50 μm for standard pictures; scale line = 175 μm for insets.)

of asbestos caused a widespread foreign body reaction in the peritoneal cavity. Importantly, all types of asbestos used crossed the mesothelia and were present in the subserosal area with granulomatous changes. After 4 weeks, chrysotile fibers were mostly unrecognizable, but crocidolite and amosite fibers were clearly visible under microscopy. All the asbestos fibers caused iron deposition in the spleen and liver. Especially, spleen 4 weeks after chrysotile administration showed high iron deposition (Fig. 5). Furthermore, we evaluated oxidative damage in the spleen, liver and kidney via immunostaining of 8-OHdG, a

doi: 10.1111/j.1349-7006.2008.00934.x

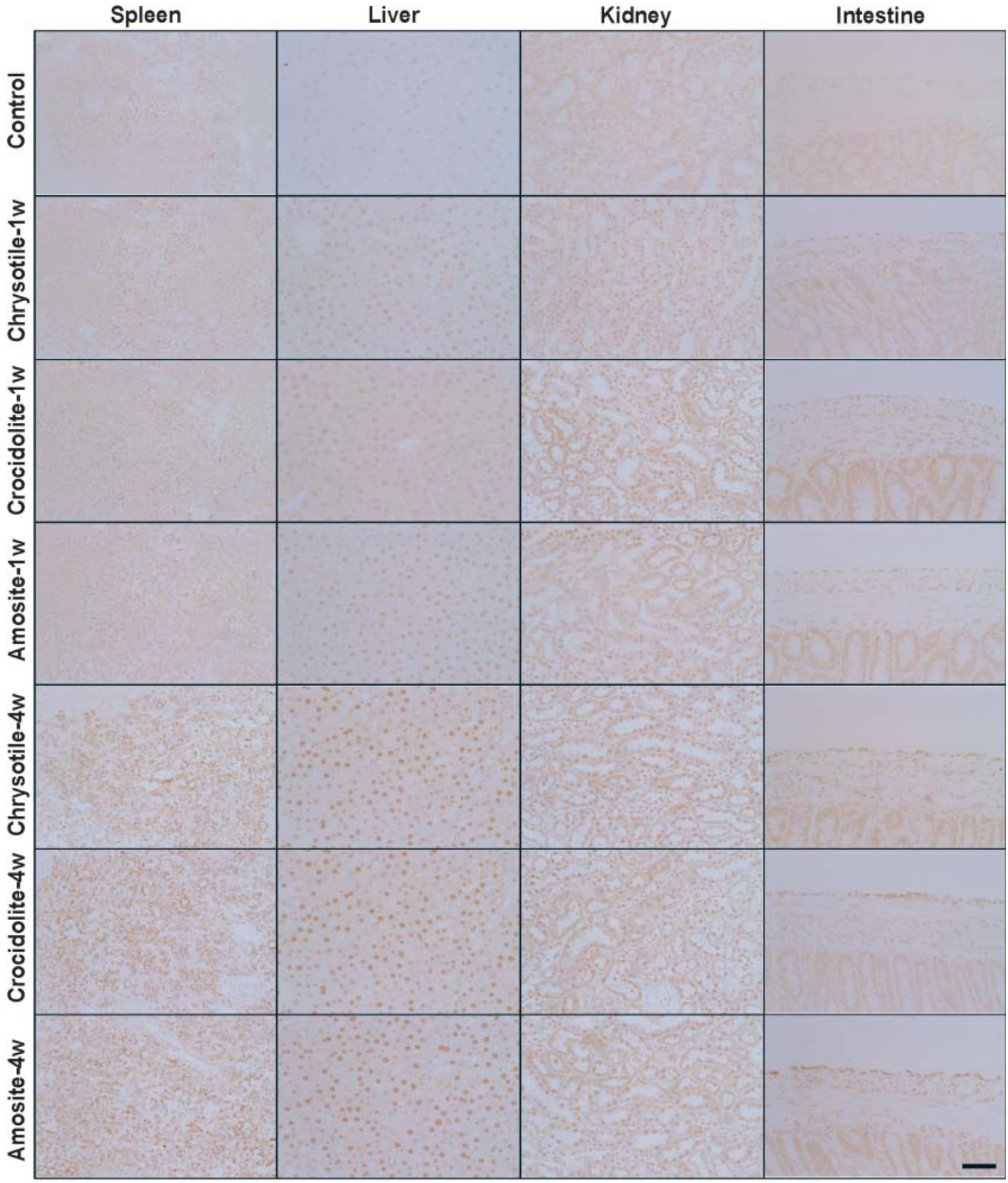

Fig. 6. Immunohistochemical analysis of 8-hydroxy-2′-deoxyguanosine (8-OHdG) after i.p. administration of asbestos. Nuclear immunopositivity was observed 1 or 4 week after i.p. asbestos administration in the spleen, liver, kidney and intestinal serosa (scale line = 50 μm).

representative oxidative stress marker.[21] One week after a single administration of crocidolite or amosite fibers, renal proximal tubules showed higher levels of 8-OHdG. In contrast, 4 weeks after a single administration of chrysotile, crocidolite or amosite fibers, renal proximal tubules showed higher levels of 8-OHdG with chrysotile fiber most intensely. Higher levels of 8-OHdG were observed also in the spleen, liver and mesothelia (Fig. 6) for all the asbestos types used.

Discussion

All kinds of asbestos were banned in Japan on 1 September 2006 (www.mhlw.go.jp/new-info/kobetu/roudou/sekimen/hei/dL/hou06-257c.pdf), but Japan nevertheless has many people at high risk for developing asbestos-induced carcinogenesis due to a prior history of asbestos exposure. In this situation, elucidation of the carcinogenic mechanism is mandatory to develop novel techniques for diagnosing asbestos-associated, early stage cancers and to develop preventive strategies for high-risk people. Oxidative DNA damage has been reported to be associated with carcinogenesis.[15,25] In the present paper, we not only re-evaluated the catalytic activities of UICC asbestos fibers for the generation of free radicals but also identified several novel characteristics of these fibers in asbestos-induced oxidative DNA damage.

The electron microscopic morphology of three kinds of UICC asbestos fibers and the metal analysis results were the same as previously described by other investigators.[9,26] The characteristics were high content of iron in crocidolite and amosite fibers (Fig. 1b). Both fibers contained ferric and ferrous iron whereas amosite contained more ferrous iron.[16] In a simple ESR condition of asbestos suspension and H_2O_2, amosite was the strongest catalyst for the generation of hydroxyl radicals, suggesting that surface ferrous iron plays an important role. We also evaluated the modifiers of these reactions. We used four different synthetic iron chelators, NTA, ethylenediaminetetraacetic acid (EDTA), DTPA and desferal, which interact with iron at three, four, five or six coordination sites, respectively, with different stability constants.[27] NTA significantly enhanced the reaction for all the asbestos fibers whereas DTPA and desferal inhibited the reaction (Fig. 1d). The results were consistent with a previous report for ferric iron solution and H_2O_2.[27] These results suggest that asbestos-induced carcinogenesis in animals will be promoted by the presence of NTA. Studies are in progress to prove this hypothesis. In the case of only amosite, EDTA was highly inhibitory. Eight natural iron chelators were slightly inhibitory. Citrate was markedly inhibitory only for amosite. These results may be explained by the steric hindrance of surface reactive ferrous iron.

We also used ESR to study RAW264.7 macrophage cells (Fig. 2e). In the cases of crocidolite and amosite, hydroxyl radicals were detected without the addition of H_2O_2. The addition of H_2O_2 markedly enhanced the ESR signals, suggesting that crocidolite and amosite fibers were within the cell. Interestingly, the toxicity of chrysotile for RAW264.7 was not necessarily associated with oxidative stress (Fig. 2a).

This study for the first time uses time-lapse video microsopy to observe the engulfment of asbestos fibers by a variety of cultured cells (Fig. 3). Surprisingly, not only phagocytic cells, but also other kinds of cells such as mesothelial cells and adenocarcinoma cells took up asbestos fibers. It is notable that asbestos fibers with shorter lengths and larger diameters were taken up faster, and that the asbestos fibers eventually reached nuclei after passing through the cytoplasm. Engulfment of the asbestos fibers was associated with oxidative stress (Fig. 3). The cells which engulfed a huge number of asbestos fibers would probably die, but some cells survive resulting in specific genetic alterations. It would be interesting to know whether a specific receptor is involved in the intake of asbestos fibers. We believe from the video files that asbestos fibers are not just physically sticking into the cytoplasm. Based on these results, we are currently searching for proteins that specifically react with each asbestos fiber.

We performed the *in vitro* experiments using supercoiled plasmid DNA to evaluate the sequence specificity of DNA DSB. The results of the strand breaks were consistent with the data from the ESR study. Only crocidolite and amosite fibers caused DSB. In the case of both fibers, repetitive sequences and consecutive C:G sequences were major targets for DSB. Homozygous deletion of the $p16^{INK4A}$ tumor suppressor gene is frequently observed in asbestos-induced mesothelioma in humans.[28–30] Our data would be helpful for analyzing the pathogenic process associated with homozygous deletions.

Finally, we performed i.p. administration of asbestos fibers to analyze general pathology of the disease. This is a different situation from the asbestos-exposed humans. However, we have chosen this because: (i) experiments of asbestos inhalation would introduce new risks for researchers; (ii) it is well established that i.p. administration of asbestos fibers including chrysotile causes peritoneal mesothelioma;[31–34] and (iii) the presence of a variety of organs in the peritoneal cavity make it an attractive system for evaluating many organs at the same time. The foreign body reaction was stronger at 1 week than at 4 weeks after a single administration of asbestos (Fig. 5). In all the cases, iron deposition was observed both in the spleen and liver (Fig. 5), but especially in spleen 4 weeks after chrysotile administration. This is probably associated with the hemolytic action of chrysotile which was previously reported.[35] It is interesting to note that not only the spleen but also the liver and kidney are oxidatively stressed 4 weeks after administration of each asbestos fiber type (Fig. 6). This clearly means that asbestos fibers *in vivo* present a more complicated pathology than in the simpler *in vitro* system.

In conclusion, iron as a component of asbestos or as a consequence of asbestos-induced pathology can be one of the major candidates for carcinogenic mechanisms because iron overload has been recognized as carcinogenic.[14] Iron chelators modify the asbestos-induced pathology. Thus, some of the iron chelators may work for preventive intervention. Asbestos enters not only the cytoplasm, but also the nuclei of affected cells. Crocidolite and amosite show an affinity for repetitive sequences or G:C sequences as the targets of DNA DSB. In spite of the current and previous studies, why mesothelial cells are the primary targets in the asbestos-induced carcinogenesis is not fully explained. Based on the present results of i.p. injection, it may be necessary to reassess the animal carcinogenesis experiments and also human epidemiological data on other cancers, including liver, kidney and spleen in people with a prior history of asbestos exposure.

Acknowledgments

This work was supported in part by a MEXT grant (Special Coordination Funds for Promoting Science and Technology), a Grant-in-Aid for Cancer Research from the Ministry of Health, Labor and Welfare of Japan, and a Grant-in-Aid from the Ministry of Education, Culture, Sports, Science and Technology of Japan.

References

1 Roggli VL, Oury TD, Sporn TA (eds). *Pathology of Asbestos-Associated Diseases*. New York: Springer Verlag, 2004.
2 Dadson RF, Hammnar SP (eds). *Asbestos. Risk Assessment, Epidemiology, and Health Effects*. Boca Raton, FL: CRC Press, Taylor & Francis Group, 2006.
3 79 Kubota workers killed by asbestos over 26 years. *Daily Yomiuri* 2005; 30 June.
4 Asbestos 'silent time bomb' feared/Revelations of workers' deaths leave residents near plants wondering who's next. *Daily Yomiuri* 2005; 7 Jul.
5 Wagner JC, Sleggs CA, Marchand P. Diffuse pleural mesothelioma and asbestos exposure in North Western Cape Province. *Br J Ind Med* 1960; **17**: 260–71.
6 Spirtas R, Heineman E, Bernstein L *et al*. Malignant mesothelioma: attributable risk of asbestos exposure. *Occup Environ Med* 1994; **51**: 804–11.
7 Edwards J, Abrams K, Leverment J, Spyt T, Waller D, O'Byrne K. Prognostic factors for malignant mesothelioma in 142 patients: validation of CALGB and EORTC prognostic scoring systems. *Thorax* 2000; **55**: 731–5.
8 Robinson B, Lake R. Advances in malignant mesothelioma. *N Engl J Med* 2005; **353**: 1591–603.

doi: 10.1111/j.1349-7006.2008.00934.x

9 Kamp DW, Graceffa P, Pryor WA, Weitzman SA. The role of free radicals in asbestos-induced diseases. *Free Radic Biol Med* 1992; **12**: 293–315.
10 McDonald A, McDonald J, Pooley F. Mineral fibre content of lung in mesothelial tumours in North America. *Ann Occup Hyg* 1982; **26**: 417–22.
11 Wang N, Jaurand M, Magne L, Kheuang L, Pinchon M, Bignon J. The interactions between asbestos fibers and metaphase chromosomes of rat pleural mesothelial cells in culture. A scanning and transmission electron microscopic study. *Am J Pathol* 1987; **126**: 343–9.
12 Jin M, Sawa H, Suzuki T *et al*. Investigation of simian virus 40 large T antigen in 18 autopsied malignant mesothelioma patients in Japan. *J Med Virol* 2004; **74**: 668–76.
13 Aoe K, Hiraki A, Murakami T *et al*. Infrequent existence of simian virus 40 large T antigen DNA in malignant mesothelioma in Japan. *Cancer Sci* 2006; **97**: 292–5.
14 Toyokuni S. Iron-induced carcinogenesis: the role of redox regulation. *Free Radic Biol Med* 1996; **20**: 553–66.
15 Toyokuni S. Molecular mechanisms of oxidative stress-induced carcinogenesis: from epidemiology to oxygenomics. *IUBMB Life* 2008; **60**: 441–7.
16 Kohyama N, Shinohara Y, Suzuki Y. Mineral phases and some reexamined characteristics of the International Union Against Cancer standard asbestos samples. *Am J Ind Med* 1996; **30**: 515–28.
17 Kawabata T, Awai M, Kohno M. Generation of active oxygen species by iron nitrilotriacetate (Fe-NTA). *Acta Med Okayama* 1986; **40**: 163–73.
18 Toyokuni S, Masumizu T, Ozeki M *et al*. An electron spin resonance study on alkylperoxyl radical in thin-sliced renal tissues from ferric nitrilotriacetate-treated rats: the effect of alpha-tocopherol feeding. *Free Radic Res* 2001; **35**: 245–55.
19 Tanaka T, Akatsuka S, Ozeki M, Shirase T, Hiai H, Toyokuni S. Redox regulation of annexin 2 and its implications for oxidative stess-induced renal carcinogenesis and metastasis. *Oncogene* 2004; **23**: 3980–9.
20 Toyokuni S, Tanaka T, Hattori Y *et al*. Quantitative immunohistochemical determination of 8-hydroxy-2′-deoxyguanosine by a monoclonal antibody N45.1: its application to ferric nitrilotriacetate-induced renal carcinogenesis model. *Lab Invest* 1997; **76**: 365–74.
21 Toyokuni S. Reactive oxygen species-induced molecular damage and its application in pathology. *Pathol Int* 1999; **49**: 91–102.
22 Goldman L, Cutrone E, Kotenko S, Krause C, Langer J. Modifications of vectors pEF-BOS, pcDNA1 and pcDNA3 result in improved convenience and expression. *Biotechniques* 1996; **21**: 1013–15.
23 Toyokuni S, Sagripanti J-L. DNA single- and double-strand breaks produced by ferric nitrilotriacetate in relation to renal tubular carcinogenesis. *Carcinogenesis* 1993; **14**: 223–7.
24 Toyokuni S, Sagripanti JL. Induction of oxidative single- and double-strand breaks in DNA by ferric citrate. *Free Radic Biol Med* 1993; **15**: 117–23.
25 Toyokuni S, Akatsuka S. Pathological investigation of oxidative stress in the postgenomic era. *Pathol Int* 2007; **57**: 461–73.
26 Hardy JA, AEA. Iron in asbestos chemistry and carcinogenicity. *Chem Rev* 1995; **95**: 97–118.
27 Toyokuni S, Sagripanti JL. Iron-mediated DNA damage: sensitive detection of DNA strand breakage catalyzed by iron. *J Inorg Biochem* 1992; **47**: 241–8.
28 Xio S, Li D, Vijg J, Sugarbaker D, Corson J, Fletcher J. Codeletion of p15 and p16 in primary malignant mesothelioma. *Oncogene* 1995; **11**: 511–5.
29 Cheng J, Jhanwar S, Klein W *et al*. p16 alterations and deletion mapping of 9p21-p22 in malignant mesothelioma. *Cancer Res* 1994; **54**: 5547–51.
30 Usami N, Fukui T, Kondo M *et al*. Establishment and characterization of four malignant pleural mesothelioma cell lines from Japanese patients. *Cancer Sci* 2006; **97**: 387–94.
31 Bolton R, Davis J, Donaldson K, Wright A. Variations in the carcinogenicity of mineral fibres. *Ann Occup Hyg* 1982; **26**: 569–82.
32 Suzuki Y, Kohyama N. Malignant mesothelioma induced by asbestos and zeolite in the mouse peritoneal cavity. *Environ Res* 1984; **35**: 277–92.
33 Davis J, Addison J, Bolton R, Donaldson K, Jones A, Smith T. The pathogenicity of long versus short fibre samples of amosite asbestos administered to rats by inhalation and intraperitoneal injection. *Br J Exp Pathol* 1986; **67**: 415–30.
34 Davis J, Addison J, Bolton R, Donaldson K, Jones A. Inhalation and injection studies in rats using dust samples from chrysotile asbestos prepared by a wet dispersion process. *Br J Exp Pathol* 1986; **67**: 113–29.
35 Ottolenghi A, Joseph L, Newman H, Stephens R. Interaction of erythrocyte membranes with particulates. *Environ Health Perspect* 1983; **51**: 253–6.

Supporting Information

Additional Supporting Information may be found in the online version of this article:

File 1. RAW264.7 cells were exposed to crocidolite.

File 2. MeT5A cells were exposed to crocidolite.

File 3. FRCC562 cells were exposed to crocidolite.

File 4. HeLa cells were exposed to crocidolite.

Please note: Wiley-Blackwell are not responsible for the content or functionality of any supporting materials supplied by the authors. Any queries (other than missing material) should be directed to the corresponding author for the article.